Response Parameters that Control the Service, Safety and Collapse Performances of a 253 m Tall Concrete Core Wall Building in Istanbul

Erhan Budak
Middle East Technical University: Orta Dogu Teknik Universitesi
Haluk Sucuoglu (sucuoglu@metu.edu.tr)
METU: Orta Dogu Teknik Universitesi https://orcid.org/0000-0003-4475-8182
Ozan Cem Celik
Middle East Technical University: Orta Dogu Teknik Universitesi

Research Article

Keywords: Tall building, Core wall, Coupling beams, Design overstrength, Seismic performance, Collapse spectrum

Posted Date: January 27th, 2022

DOI: https://doi.org/10.21203/rs.3.rs-1291240/v1

Response Parameters that Control the Service, Safety and Collapse Performances of a 253 m Tall Concrete Core Wall Building in Istanbul

Erhan Budak, Halûk Sucuoğlu*, Ozan Cem Celik

Department of Civil Engineering, Middle East Technical University, Ankara, Turkey

Abstract

Seismic performance of a 253 m tall reinforced concrete core wall building in Istanbul, designed according to performance-based seismic design principles, is assessed for determining the response parameters that control the serviceability, safety and collapse performance limit states. Serviceability performance is evaluated under the 50-year wind and 43-year earthquake whereas safety performance is assessed under the 2475-year earthquake. Collapse performance is elaborated through incremental dynamic analysis. Our study revealed that the service performance is controlled by the maximum interstory drift limits specified for wind loads, and safety performance is controlled by the flexural steel strain limits of coupling beams. Collapse occurs in two consecutive stages: flexural collapse of coupling beams, followed by crushing of concrete at critical shear wall segments. *Collapse spectra* are defined for these two collapse limit states. Collapse spectra can be extrapolated from the 2475-year maximum considered earthquake (MCE) spectrum provided that the prevailing inelastic mechanisms are similar under the MCE and collapse ground motions. The building displays a significantly higher seismic performance at all performance levels, which is primarily attributed to the overstrength due to the limitation of axial stresses on vertical members under design earthquake load combination. The annual frequency of the mean earthquake ground motions that leads to incipient collapse is determined as $8 \cdot 10^{-5}$, which is significantly lower than the annual frequency of 2475-year ground motions.

Keywords: Tall building, Core wall, Coupling beams, Design overstrength, Seismic performance, Collapse spectrum

1 Introduction

The population of tall buildings, with a significant portion in regions of high seismicity, is steadily increasing in the world. Design of tall buildings under gravity and wind loading in non-seismic regions is well developed and has a history longer than a century. However, tall building boom in seismic regions is a fairly new phenomenon. In Istanbul, the number of buildings taller than 100 m has exceeded 200 (Erdik et al. 2003; Odabasi et al. 2021). Tall buildings are unique in architectural and structural features when compared to ordinary multistory buildings. These differences become more prominent in seismic zones where seismicity and unique dynamic building characteristics dominate structural design. Past seismic design practices and existing prescriptive procedures may not promote the desired behavior for tall buildings under earthquake excitations. Hence, chapters devoted particularly to tall buildings are included in the recent seismic design codes, or pertinent guidelines have been published (AFAD 2018a; LATBSDC 2017; PEER 2017; SEAONC 2007).

Although there are several studies on the seismic performance assessment of tall buildings, they are mostly carried out on analytical archetype models. Research studies on the existing constructed tall buildings aiming at determining the relations between the adopted seismic design criteria and the achieved seismic performances are limited (Wang et al. 2017; Bilotta et al. 2018; Korista et al. 1997). The focus of this study is to investigate and identify the critical structure-specific or member-specific response parameters that significantly control the serviceability, safety and collapse performances of a 253 m tall concrete core wall building, which was recently constructed in Istanbul. Seismic design was based on state-of-the-art guidelines and practices prevailing during the planning stage of the project in 2016 (Budak et al. 2018).

It is expected that the findings of this study further improve the understanding of the seismic performance of tall concrete core wall buildings designed by professional practitioners under strong earthquake excitations. Along this perspective, determining the key response characteristics that dominate the limit states, the inherent sources of overstrength, and the intensities and annual occurrence frequencies of earthquake ground motions leading to local and global collapse are the key aspects of the presented study.

* Corresponding author: sucuoglu@metu.edu.tr

2 Building characteristics

The building is a 253 m tall, 62-story reinforced concrete (RC) building, including eight podium floors below the ground level, the ground (G) floor and 53 floors above the ground level. The typical floor-to-floor height is 4.0 m, whereas the height of the ground story is 8.75 m and the total height of the podium stories is 31.75 m. The building was designed for mixed office and residential use. Figure 1 shows building section, typical podium floor plan and the view of the building from the northeast corner during its construction. The parallelogram footprint was necessitated due to the plan optimization based on the available land geometry, which causes additional torsional effects under lateral loading.

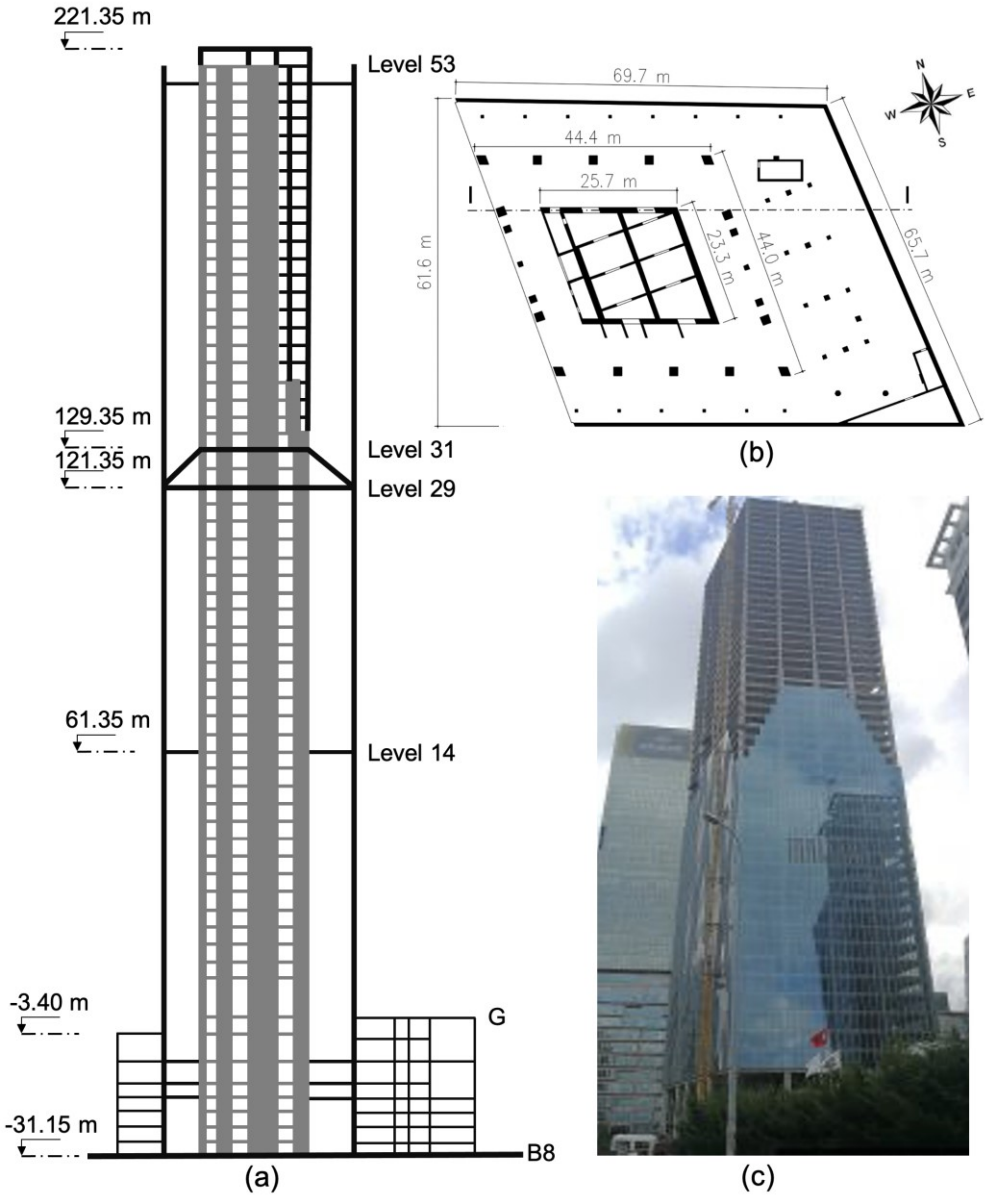

Fig. 1 a Building section I-I, **b** typical podium floor plan and **c** construction view from the northeast corner

Typical floor plan of the tower is shown in Fig. 2. The thickness of the main segments of the core shear walls at the lower stories are 1.00 m for P1–P8 and 1.10 m for P22 and P25. Thicknesses gradually reduce in four stages to 0.60 m at the upper stories. P24 is 0.80 m thick at the lower half of the tower and 0.60 m at the upper half. Other wall segments are 0.40 m thick throughout the height of the building.

At the eight podium stories, square RC columns are 1.50–1.60 m in size under the tower except at the top podium story and 0.90 m elsewhere. Above the top podium floor level, up to floor 27, square composite columns with encased HD 400 steel sections are 1.00–1.10 m in size, whereas square RC columns are 0.60–1.00 m in size at the upper stories.

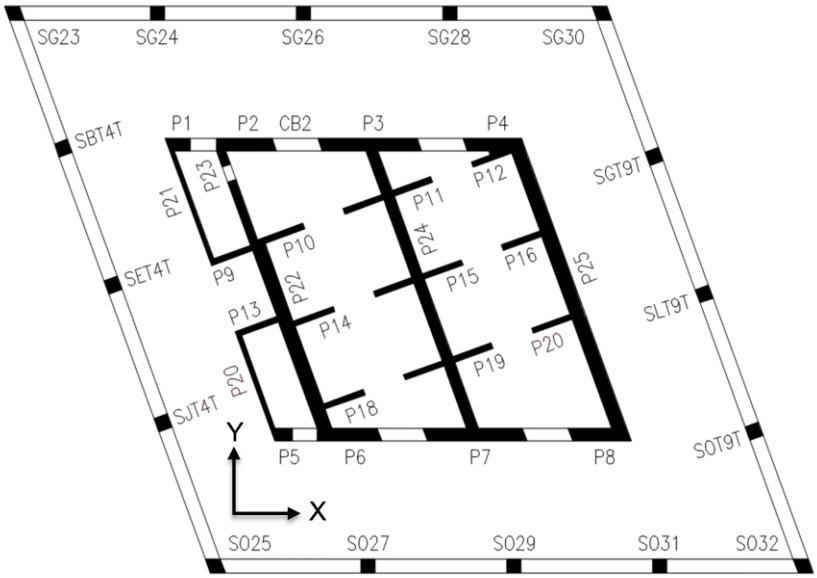

Fig. 2 Typical tower floor plan

Three pairs of two-story tall diagonal RC outrigger braces in the North-South (N-S; Y) direction and two pairs of similar outriggers in the East-West (E-W; X) direction were incorporated between floors 29 and 31 (Fig. 1a) to reduce the interstory drifts and bending moments in the core wall under wind and earthquake effects. The outrigger members are 1.20 m deep and 0.75 m wide.

The tower floors are composed of 0.25 m thick conventional RC flat plates. Slab thickness at the upper podium level was selected as 0.40 m to control the backstay effects, and reduces to 0.30 m at the lower podium floors. The perimeter beams are 0.60 m deep and 1.00 m wide.

There are two types of coupling beams at each story. One type is 2.2 m long and 0.85 m deep, and the other type is 3.3 m long and 1.12 m deep. The clear span to depth ratios are 2.6 and 2.9, respectively. Their thicknesses conform to the thickness of adjacent walls.

The building has a 4.8 m thick mat foundation under the tower, which gradually reduces to 3.5 m, 2.0 m and 1.5 m under the podium floors. It is located on stiff soil (Soil Group ZC; MPWS 2007), equivalent to NEHRP Type C (FEMA 2020), where the average shear wave velocity in the upper 30 m of the site profile, V_{s30}, is 500 m/s.

Concrete characteristic strength, f_{ck}, is 60 MPa at the core walls, coupling beams and tower columns, and 40 MPa at all other members. Characteristic yield strength of reinforcing steel, f_{yk}, is 420 MPa whereas yield strength of structural steel, f_y, in composite members is 460 MPa.

3 Structural design

Structural design was completed in 2016. Hence, seismic codes and standards prior to 2016 were considered in design. The structural system of the tower is composed of a core wall connected to peripheral columns and beams with flat plates. Wind tunnel tests were carried out in order to determine the design wind load distributions (ASCE 2012; WTG 1996; European Committee for Standardization 2005).

Two different performance targets were considered in seismic design (SEAONC 2007; PEER 2010): operational performance under an earthquake with a return period of 43 years (service-level earthquake; SLE) and collapse prevention performance under 2475-year earthquake (maximum considered earthquake; MCE) ground motions. Structural design and detailing was based on response spectrum analysis under the SLE. Capacity shears were employed in the shear design of ductile members. The dominant design load combination that includes seismic action for the SLE is

$$D + 0.25L + E_h \tag{1}$$

where D is the dead load, L is the live load and E_h is the horizontal design earthquake load ($E_h = \pm E_{\mathrm{X}} \pm 0.3\, E_{\mathrm{Y}}$); E_{X} and E_{Y} are the earthquake actions obtained from response spectrum analysis along the X and Y directions, respectively. The design approach with pertinent limitations imposed are summarized in the following.

3.1 Axial load limits

Maximum permitted normalized compressive stresses acting on RC members are $N_d/A_c f_{ck} < 0.40$ for concrete columns and $N_d/A_c f_{ck} < 0.25$ for shear walls, where N_d is the axial load demand calculated under the design load combination in Eq. (1) and A_c is the gross area of the concrete cross section. For composite columns, the maximum value of the axial load is $N_d < 0.4N_{ro}$ when N_d is calculated from the $1.2D + L + E_h$ load combination (MPWS 2007), and $N_d < 0.8N_r$ when N_d is calculated from the $1.4D + 1.6L$ combination (TSI 2000), where N_{ro} and N_r are the axial load capacities of the composite columns:

$$N_{ro} = 0.85A_{co}f_{ck} + A_s f_{yk} + A_a f_y \tag{2}$$

$$N_r = 0.85A_{co}\, f_{ck}/1.5 + A_s\, f_{yk}/1.15 + A_a\, f_y/1.1 \tag{3}$$

where A_{co} is the net concrete area, A_s is the longitudinal reinforcement area and A_a is the area of the steel section.

3.2 Reinforcement limitations

Limitations on reinforcement were dictated by the existing design codes (MPWS 2007; TSI 2000; ACI 2014). Longitudinal reinforcement ratio ρ for RC columns is $0.01 < \rho < 0.04$. For composite columns, the area of the steel section should exceed ρ_s = 0.04 times the gross section area. In the web region of shear walls, $\rho > 0.0025$ of the web cross-sectional area whereas in the confined end regions of shear walls, $\rho > 0.0020$ of the total wall area within the critical height region and $\rho > 0.0010$ above the critical height region. For beams, the longitudinal tensile reinforcement ratio ρ should satisfy $0.6\, f_{ctk}/f_{yk} < \rho < 0.02$ as well as $\rho < 0.85\rho_b$. Here, f_{ctk} is the characteristic tensile strength of concrete and ρ_b is the balanced tensile reinforcement ratio. Further detailing requirements are not repeated here as they are common in the existing design codes.

3.3 Flexural design

Design bending moments for columns, core walls and beams were determined from the response spectrum analysis under the load combination in Eq. (1). Design bending moment distributions for the core walls were modified to consider dynamic amplification (Moehle et al. 2012), in order to ensure that plastic hinging only occurs at the designated critical sections of the walls. Critical wall sections in this building where maximum bending moments develop are at the base of the ground story and above the podium floor.

3.4 Shear design

Design shear forces for beams and columns are the capacity shear forces, which are based on the flexural strength of the end sections. Design shear forces in core walls at any section were calculated from

$$V_e = \left(M_{p,t}/M_{d,t}\right)V_d \tag{4}$$

where $M_{p,t}$ is the moment capacity at the critical section of the core wall, and $M_{d,t}$ is the bending moment and V_d is the shear force calculated at the critical section under the SLE. However, these forces should not exceed $3.5V_d$. Critical wall height is 1/6 of the total wall height above the critical section (MPWS 2007).

3.5 Performance limits under the SLE and wind

Column, beam and core wall moment demand-to-capacity ratios (DCRs) for deformation controlled actions should not exceed 1.5 under the design load combination given in Eq. (1). Similarly, shear DCRs of these members should not exceed 0.7 in order to suppress the shear mode of failure. Expected material strengths were employed for calculating the capacities, which are $1.3f_{ck}$, $1.17f_{yk}$ and $1.1f_y$ for concrete, reinforcing steel and structural steel, respectively (LATBSDC 2017).

Interstory drift ratio (IDR) is limited to 0.5% under the SLE (PEER 2010; LATBSDC 2017) for ensuring that the system remains essentially linear elastic. Furthermore, IDR is limited to 1/500 (0.2%) under 50-year wind load (Smith 2011; Arup Inc. 2013).

3.6 Performance limits under the MCE

Mean maximum transient IDR obtained under the MCE ground motions ensemble and the maximum IDR under each ground motion are limited to 3.0% and 4.5%, respectively (PEER 2010; LATBSDC 2017). The mean shear DCRs in all members should not exceed 1.0 under the MCE ground motions.

Performance of the building is deemed satisfactory if the calculated compressive strains for confined concrete are less than 0.010 and reinforcing steel tensile strains are less than 0.030 for columns, core wall segments, beams and coupling beams (PEER 2010).

4 Analytical models

A 3-D linear elastic finite element model of the building was developed for calculating the design forces and deformations under the load combination in Eq. (1) using ETABS software (CSI 2011). Shell elements were employed for the shear walls and slab members whereas the column and beam members were represented by frame elements. Gross section properties were reduced by effective section stiffness multipliers for the SLE and wind loading: 0.90 for columns, 0.75 for shear walls, 0.70 for perimeter beams, 0.50 for slabs and 0.30 for coupling beams (PEER 2010).

An eigenvalue analysis of the linear elastic structural model was performed. Table 1 provides the natural vibration periods and effective modal masses for the first six vibration modes. Rotation is apparently dominant in the third and fifth modes.

Table 1 Dynamic properties

Mode	Period (s)	Modal Mass Ratio (%)	
		E-W	N-S
1	6.0	30	22
2	4.1	23	28
3	3.3	0	0
4	1.7	7	4
5	1.3	0	1
6	0.9	3	11

A 3-D inelastic dynamic model was further developed for nonlinear analysis under the MCE and collapse ground motions using Perform3D software (CSI 2016). Fiber-type shell elements and lumped plasticity models were used for shear walls and frame members, respectively, responding beyond the linear elastic range (PEER 2010; Wallace 2007; Zekioglu et al. 2007).

Previous studies show that the use of typical concrete material models (e.g., Mander et al. 1988) in modeling shear walls lead to inaccurate simulation of cyclic responses and drift capacities when compared with the experimental counterparts. Hence, regularized concrete material response, modifying post peak stress-strain response based on concrete fracture energy, was used for the fiber-type shell elements in order to capture the cyclic responses and drift capacities accurately (Pugh et al. 2015; Lowes et al. 2016). Steel bars in tension were represented by the elasto-plastic steel model with 1% strain hardening, whereas steel bars in compression were represented by the simple buckling steel model proposed by Pugh et al. (2015) for simulating the wall response until concrete reaches residual compressive strength. Stress-strain relations for concrete in compression and steel in tension are presented in Fig. 3.

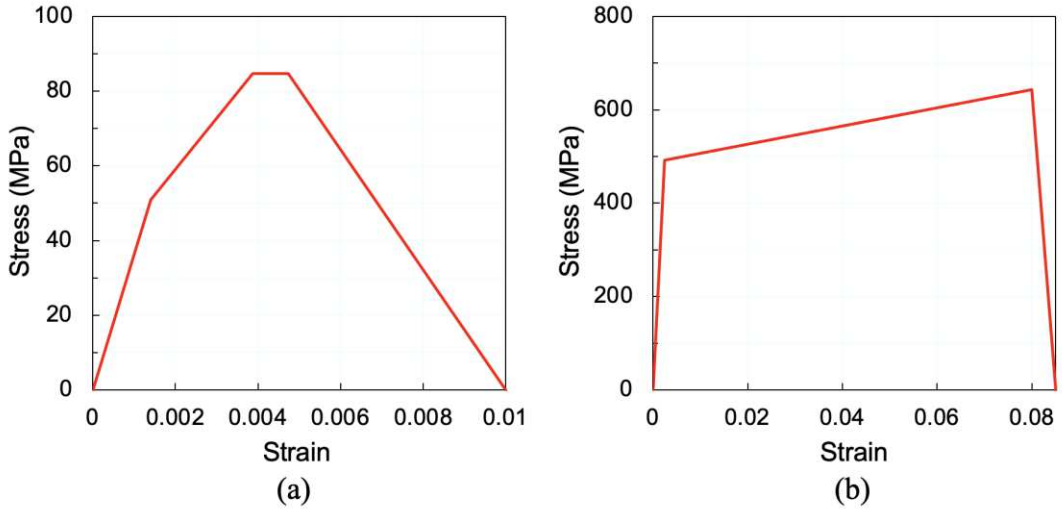

Fig. 3 a Concrete and **b** steel material models

Quasi-elastic frame elements were employed for the column and beam members responding in the linear elastic range. Effective section stiffness multipliers were 0.70 for columns, 0.35 for beams and 0.20 for coupling beams. For inelastic beam properties, piecewise linear moment-curvature relationships were defined along the hinge lengths, which are assumed as one half of the cross-section depth, at both ends of all beam elements. Moment-curvature relations were derived by using the Mander model (Mander et al. 1988) for unconfined and confined concrete and the elasto-plastic model in Fig. 3b for steel. Column elements were modeled with P-M-M hinges. Geometric nonlinearity was also taken into account in the 3-D analytical model. Slab members in the nonlinear model were idealized as equivalent beam type elements per ASCE 41-13 (ASCE 2014). The diagonal outrigger members are tension-compression members; hence, their nonlinear response was idealized by a nonlinear concrete strut in compression (Mander et al. 1988) and by an elasto-plastic steel bar with 1% strain hardening in tension.

5 Probabilistic seismic hazard analysis and strong ground motions

A site-specific probabilistic seismic hazard analysis (PSHA) was performed to develop the response spectra for hazard levels of 50% probability of exceedance (PE) in 30 years and 2% PE in 50 years, which respectively correspond to mean recurrence intervals of 43 and 2475 years, i.e. the SLE and MCE. The PSHA methodology relies on the historical and recorded seismicity as well as neotectonic faulting structure of the Istanbul region and ground motion modeling (Akkar 2014).

Figure 4a presents the 2.5% and 5% damped site-specific acceleration response spectra for the SLE and MCE hazard levels, respectively. Viscous damping ratio, ξ, is taken as 2.5% rather than the conventional 5% in obtaining the SLE spectrum, because very limited concrete cracking is expected under the SLE excitation (PEER 2017). The MCE spectrum is employed as target spectrum in selecting and scaling the 18 MCE ground motion pairs (Akkar 2014).

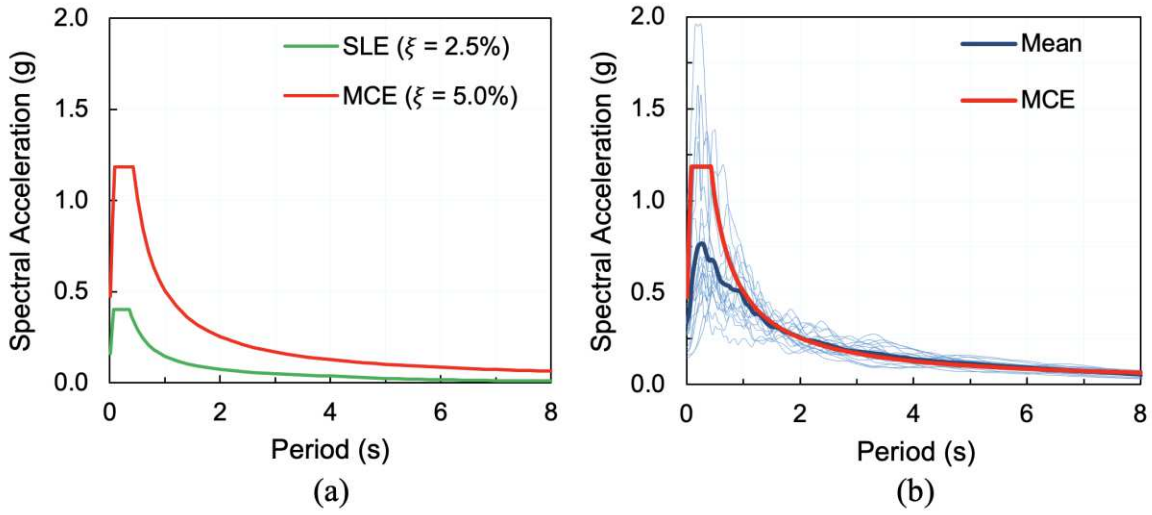

Fig. 4 a Site-specific SLE and MCE response spectra and **b** acceleration response spectra of ground motions scaled to MCE response spectrum

Deaggregation for the MCE hazard yielded the earthquakes that contribute most significantly as moment magnitude (M_w) 7.5 earthquakes occurring at epicentral distances (R_{JB}) 26–49 km. Accordingly, the strong ground motion records were selected from the PEER NGA Database (PEER 2022) with the following constraints pertaining to the construction site: $6.0 \leq M_w \leq 8.0$, $R_{JB} \leq 50$ km, and $300\ \text{m/s} \leq V_{s30} \leq 700\ \text{m/s}$. Then, ground motion amplitude scaling was carried out on the geometric mean spectrum of each pair according to the ASCE 7-16 (ASCE 2017) procedure. The seismological properties and scale factors (SF) of the ground motions are given in Table 2. Figure 4b presents the response spectra of these near fault ground motions that were scaled to match the target MCE spectrum.

Table 2 Selected acceleration records, their seismological features and scale factors

#	Event	Record	Station	M_w	R_{JB} (km)	V_{s30} (m/s)	SF
1	Landers 1992	RSN0838	Barstow	7.3	15.2	660	2.19
2	Kocaeli 1999	RSN1164	Istanbul	7.5	49.7	425	3.25
3	Landers 1992	RSN0900	Yermo Fire Station	7.3	23.6	354	1.89
4	Chi-Chi 1999	RSN1534	TCU107	7.6	16.0	409	1.11
5	Chi-Chi 1999	RSN1535	TCU109	7.6	13.1	535	0.90
6	Chi-Chi 1999	RSN1541	TCU116	7.6	12.4	493	1.26
7	Chi-Chi 1999	RSN1545	TCU120	7.6	7.4	459	1.25
8	Chi-Chi 1999	RSN1546	TCU122	7.6	9.3	476	1.21
9	Chi-Chi 1999	RSN1549	TCU129	7.6	1.8	511	1.20
10	Chi-Chi 1999	RSN1551	TCU138	7.6	9.8	653	1.32
11	Duzce 1999	RSN1611	Lamont 1058	7.1	0.2	529	3.03
12	Hector Mine 1999	RSN1762	Amboy	7.1	41.8	383	1.68
13	Chi-Chi 1999	RSN2704	CHY029	6.2	25.8	545	2.99
14	Chi-Chi 1999	RSN2708	CHY034	6.2	28.5	379	3.68
15	Chi-Chi 1999	RSN2888	TCU116	6.2	28.7	493	3.23
16	Chi-Chi 1999	RSN2893	TCU122	6.2	23.1	476	3.94
17	Cape Mendocino 1992	RSN3750	Loleta Fire Station	7.0	23.5	516	1.66
18	Chuetsu-oki 2007	RSN4848	Joetsu Ogataku	6.8	16.8	414	1.99

6 Response parameters that control the service performance level under the SLE

The target performance level for tall buildings under the SLE and 50-year wind is "operational." Hence, the response should be essentially linear elastic. This is ensured by the performance limits stated in Section 3.5, in terms of IDRs and structural member DCRs.

IDRs throughout the building height are shown in Fig. 5a, under the SLE spectrum and the 50-year wind forces in both directions. The wind forces control interstory drifts up to floor 30 (below the outrigger level) and the earthquake forces control above floor 30. However, IDRs are significantly below the 0.5% limit under the SLE, and reasonably below the 0.2% limit under the 50-year wind.

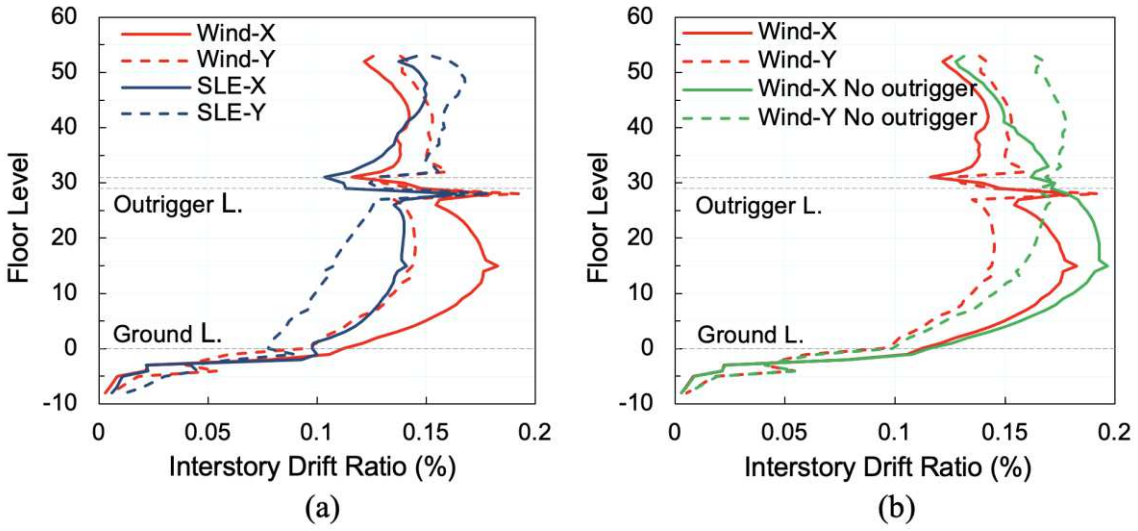

Fig. 5 a IDRs under the SLE spectrum and 50-year wind loads **b** the effect of outriggers on IDRs under 50-year wind loads

Moment and shear DCRs of selected shear wall segments are presented in Fig. 6. All DCR values are well below the moment DCR limit of 1.5 and the shear DCR limit of 0.7. Respective DCR values for the peripheral columns are much lower, maximum moment DCRs around 0.6 and shear DCRs around 0.2.

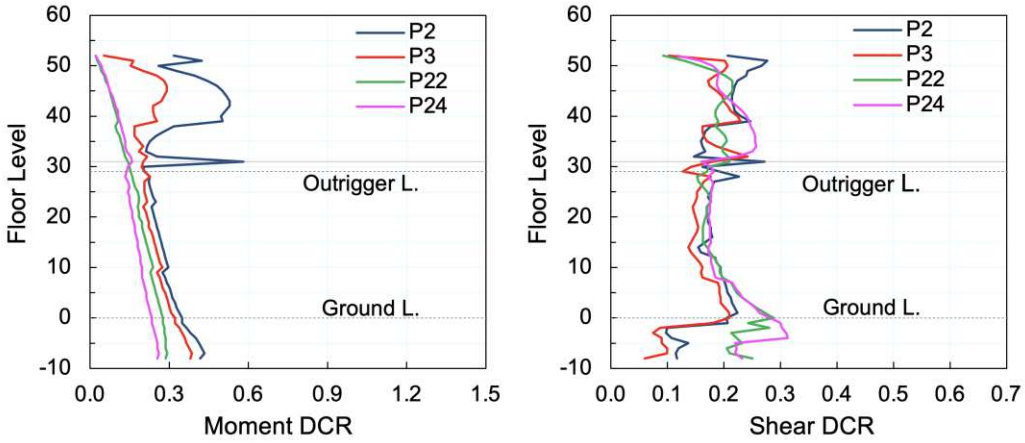

Fig. 6 Moment and shear DCRs of selected wall segments under the SLE spectrum

A comparative graphical view of the maximum DCRs for each member type and maximum IDRs throughout the building height is presented in Fig. 7 in a normalized form. The moment and shear DCRs are normalized with their respective limits of 1.5 and 0.7. Earthquake maximum IDRs are normalized with 0.5%, and wind maximum IDRs are normalized with 0.2%.

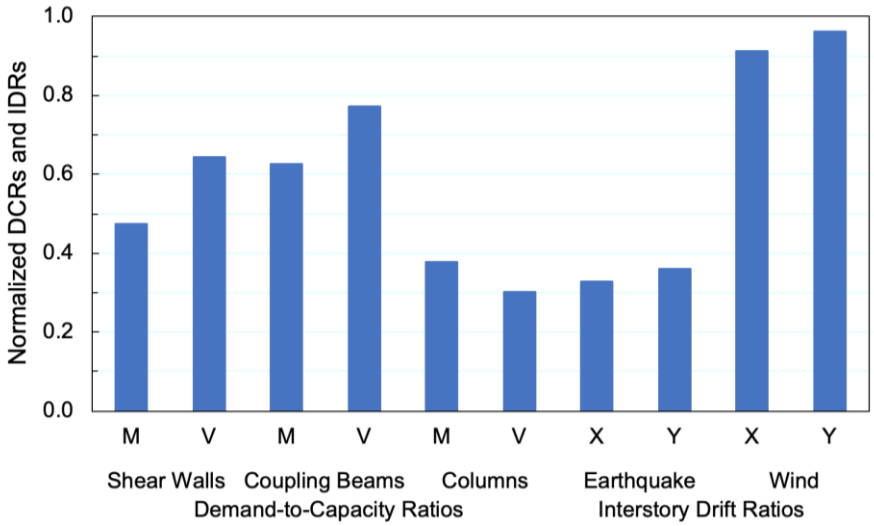

Fig. 7 Maximum normalized DCRs (M: moment, V: shear), and IDRs under the SLE spectrum and 50-year wind loads for the most critical members

The response parameter that controls the service performance level of this building is apparently the maximum IDRs under the 50-year wind. On the other hand, in seismic regions with very low wind speeds, the service performance of a core wall building would be controlled by the moment and shear DCRs of the coupling beams.

Outriggers were employed in the investigated structural system mainly for reducing the IDRs under wind loads. However, the results displayed in Fig. 5b indicate that this reduction is not significant. The 0.2% IDR limit for 50-year wind would have been satisfied without outriggers. This is perhaps due to the competent lateral stiffness of the core wall system, which is an outcome of imposing the stress limits indicated in Section 3.1. The role of outriggers might have been more prominent in the reduction of floor accelerations for comfort, but such a criterion is not imposed in tall building design (Smith 2011).

The maximum IDRs under the SLE are significantly lower than the IDR limits for service performance (Figs. 5a and 7). Hence, imposing limits on IDRs is not effective at the service performance level of a tall concrete core wall system. IDR limits may be more effective on tall steel buildings.

7 Response parameters that control the safety performance level under the MCE

The target performance level under the MCE is "collapse prevention." Hence, the response under the MCE ground motions is expected to be inelastic. This target performance is satisfied if the performance limits stated in Section 3.6, in terms of IDRs and material strains of structural members, are not exceeded.

Figure 8 presents the normalized mean material strains in the most critical members and normalized IDRs at the most critical story under the MCE ground motion pairs. Mean concrete and steel strains, ε_c and ε_s, are normalized with the MCE limits of $\varepsilon_{c,\mathrm{MCE}} = 0.010$ and $\varepsilon_{s,\mathrm{MCE}} = 0.030$, respectively, whereas mean IDRs are normalized with 3.0%. It is worth noticing that the limiting concrete strain is equal to the ultimate strain calculated for the regularized concrete model given in Fig. 3. Figure 9 presents the normalized concrete and steel strains in shear wall segments determined under each MCE ground motion pair. Likewise, maximum IDRs can be seen in Fig. 10, which shows the variation of maximum base shear forces (normalized with the building weight) against maximum IDRs in each direction, calculated under the SLE spectrum and MCE ground motions. Note that maximum base shear and IDR are not necessarily synchronous.

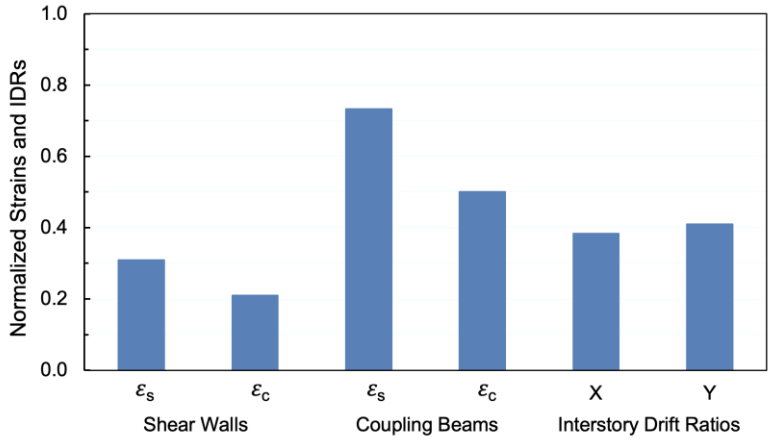

Fig. 8 Normalized mean material strains for the most critical members and normalized IDRs under MCE ground motions

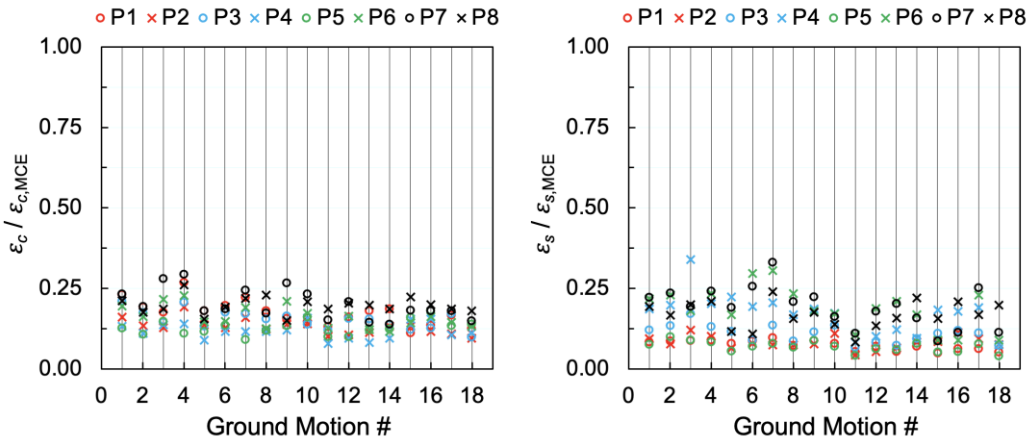

Fig. 9 Maximum normalized concrete and steel strains in shear wall segments under MCE ground motions ($\varepsilon_{c,\mathrm{MCE}} = 0.010$ and $\varepsilon_{s,\mathrm{MCE}} = 0.030$)

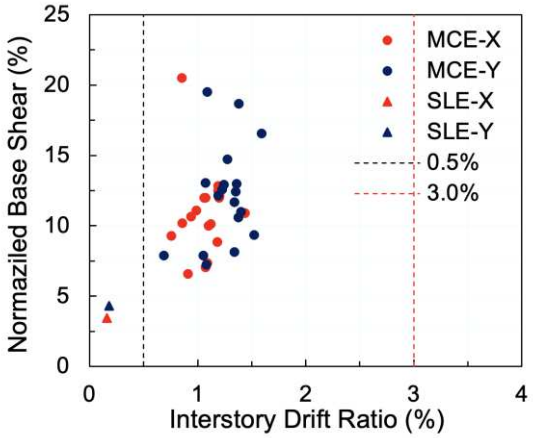

Fig. 10 Base shear vs. maximum IDR under the SLE response spectrum and MCE ground motions

The normalized mean material strains in shear wall segments shown in Fig. 9 and IDRs in Fig. 10 under the 18 MCE ground motion pairs are quite low compared to the respective MCE limits. Shear walls are effectively at the incipient yielding state, whereas the coupling beams are purely in the yielding phase during their maximum responses under the MCE ground motions, as marked on the moment-curvature diagrams of the most critical members in Fig. 11. The analyses also indicate that the peripheral columns remain linear elastic under the MCE ground motions. Therefore, Figs. 8–10 reveal that the safety performance level under the MCE is dominantly controlled by the tensile steel strains, and hence by the plastic curvatures of coupling beams.

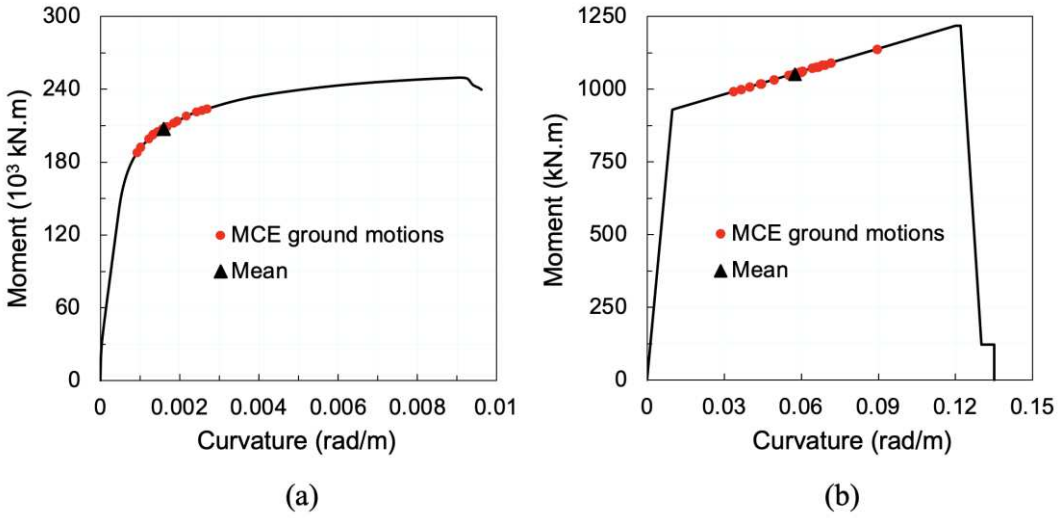

Fig. 11 Maximum curvatures at the most critical **a** shear wall (P7) and **b** coupling beam (CB2, floor 14) under MCE ground motions, marked on the moment-curvature diagrams of the respective shear wall and beam sections

8 Response parameters that control the collapse performance

Each ground motion pair is scaled upwards from the MCE level by incrementally increasing their geometric mean spectrum until collapse is achieved. Collapse occurs in two consecutive stages. In the first stage, a coupling beam fails when maximum curvature exceeds the ultimate curvature of the beam (e.g., 0.122/m for CB2 on floor 14; see Fig. 11b). Concrete and steel strains in shear walls are far from critical at this stage, as shown in Fig. 12. Note that concrete and steel strains are now normalized with the ultimate limits, ε_{cu} = 0.010 and ε_{su} = 0.080, respectively. As upward scaling continues incrementally, almost all coupling beams fail before the commencement of concrete crushing at the critical shear wall fibers. The computer algorithm permits further analysis steps with zero stiffness and strength of the failed coupling beams. In the second stage, failure occurs when concrete strain at the most critical shear wall reaches the crushing strain of 0.01. Figure 13 shows the normalized concrete and steel strains in shear wall segments at this stage under each ground motion pair.

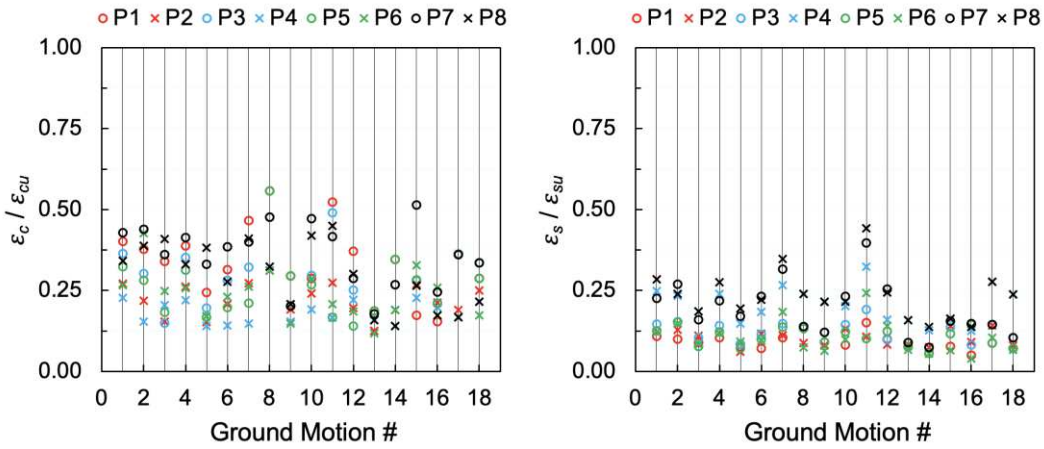

Fig. 12 Maximum normalized concrete and steel strains in shear wall segments under 18 ground motion pairs at the instant of first coupling beam failure (ε_{cu} = 0.010 and ε_{su} = 0.080)

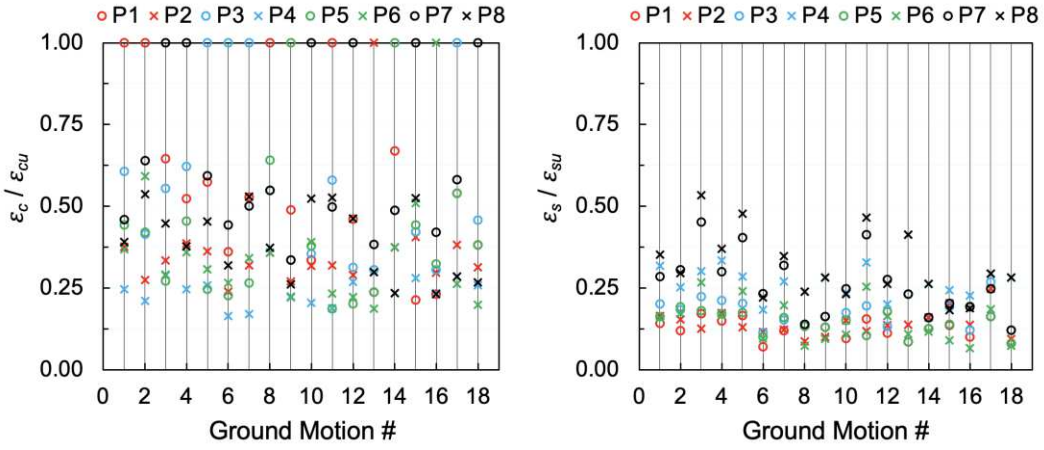

Fig. 13 Maximum normalized concrete and steel strains in shear wall segments under 18 ground motion pairs at the instant of first shear wall failure (ε_{cu} = 0.010 and ε_{su} = 0.080)

These two failure stages, identified with the first coupling beam failure and the first shear wall concrete crushing in Figs. 12 and 13, are defined as *partial collapse* and *near collapse*, respectively. The response parameters that control these two collapse stages are the coupling beam ultimate curvatures (Fig. 11b) or their corresponding tensile steel strains, and shear wall compressive concrete strains (Fig. 13a). The increase in concrete and steel strains from partial to near collapse states are clearly observed in Figs. 12 and 13. Under each ground motion, the wall segment that reaches concrete crushing first controls ultimate failure. P1, P3 and P7 are the most controlling shear wall segments (see Fig. 2). Along each vertical ground motion line in Fig. 13, as the critical wall segment approaches crushing along the degrading stress-strain segment in Fig. 3a, the other wall segments do not follow the critical one closely, which can be attributed to the redistribution of internal stresses in the core wall.

Figure 14 presents the geometric mean acceleration response spectra of the ground motion pairs scaled to the first coupling beam failure (partial collapse) and first shear wall failure (near collapse) stages. Their mean spectra are named as the *partial collapse spectrum (PCS)* and *near collapse spectrum (NCS)*. Together with the mean spectrum of ground motions scaled to the MCE spectrum, they are compared in Fig. 15a with the site specific uniform hazard spectra, which are standardized to the code spectrum format, for return periods of 43, 475 and 2475 years (i.e., the SLE, the design basis earthquake DBE and the MCE, respectively).

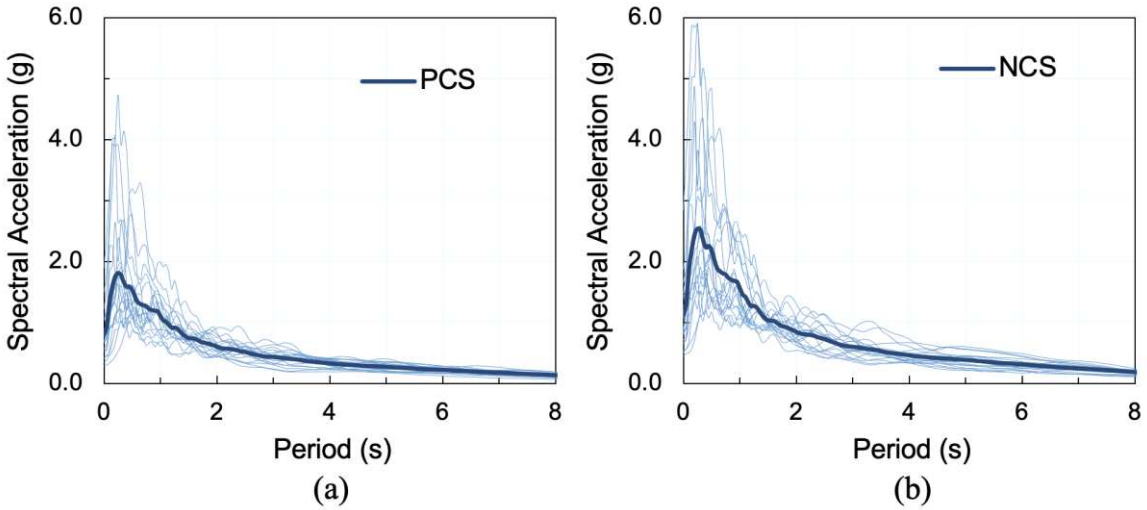

Fig. 14 Acceleration response spectra of ground motions leading to **a** partial collapse and **b** near collapse

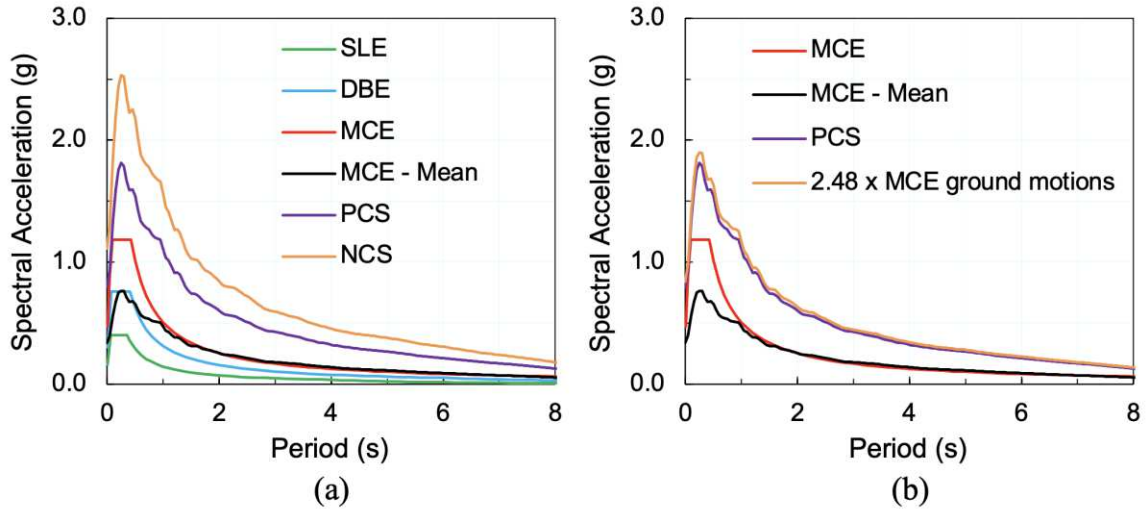

Fig. 15 Mean acceleration response spectra of MCE ground motions, partial collapse and near collapse spectra, and the standardized code spectra for 43, 475 and 2475 year return periods

9 Prediction of partial collapse spectrum from the MCE spectrum

Seismic codes and regulations for tall building design mandate nonlinear time history analysis under selected ground motion pairs scaled to the MCE spectrum. For the investigated tall concrete building, the moment-curvature response for the most critical coupling beam under each MCE scaled ground motion pair is readily available, as indicated in Fig. 11b. Under the MCE ground motions, maximum curvatures are all located on the post-elastic linear segment of the moment-curvature diagram. As the intensity of each ground motion is incrementally increased, the associated curvature point moves away from the MCE point on the post elastic linear segment until it reaches the ultimate curvature capacity of the coupling beam. The inelastic mechanism of the building does not change between these two limit states, i.e., the critical coupling beam and all others are in the post-elastic "linear" state while the shear wall members are at the incipient inelastic response state (Fig. 11a). This stable linearity from MCE to partial collapse under each ground motion for the most critical coupling beam, i.e., the one that reaches the failure state first, motivates searching for the similarity of the ratio of ground motion scale factors, and the ratio of absorbed plastic energies between the MCE and partial collapse states.

The ratio of PCS to MCE spectrum, both given in Fig. 15b, is very stable along the period axis, with a mean value of 2.35 and almost with no dispersion. The ratio of absorbed plastic energies under the post-elastic linear moment-curvature segment in Fig. 11b for a unit plastic hinge length, from yield to the MCE curvature and from yield to the end of the linear post-elastic segment, i.e., 0.122/m at incipient collapse, can be calculated for each ground motion. Their mean value is 2.48, which is sufficiently close to the spectrum scale factor 2.35 with a mere 5% difference. Consequently, if the MCE spectrum is scaled by 2.48, the PCS can be closely estimated without

carrying out an incremental dynamic analysis for each ground motion. The estimated PCS is displayed in Fig. 15b and compared with the actual PCS.

It should be noted that a similar scaling cannot be applied to the MCE spectrum for obtaining the NCS, because the inelastic mechanism of the building changes significantly between the partial collapse state (coupling beam collapse) and the near collapse state (shear wall collapse).

Figure 16 shows the seismic hazard curve in terms of spectral acceleration at the fundamental period of the building, T_1, that is constructed (Cornell et al. 2002) using the available hazard data for the building site (41.0812°N, 29.0096°E; Soil Group ZC; AFAD 2018b), which include hazard levels with mean recurrence intervals, T_r = 43, 72, 475 and 2475 years. Mean spectral acceleration values at T_1 for the ground motions that will lead to partial and near collapse of the building, i.e., 0.21g and 0.31g, respectively, cf. Fig. 14, are entered into the constructed hazard curve. The return periods of the mean partial and near collapse ground motions are estimated as 12000 and 27000 years, respectively.

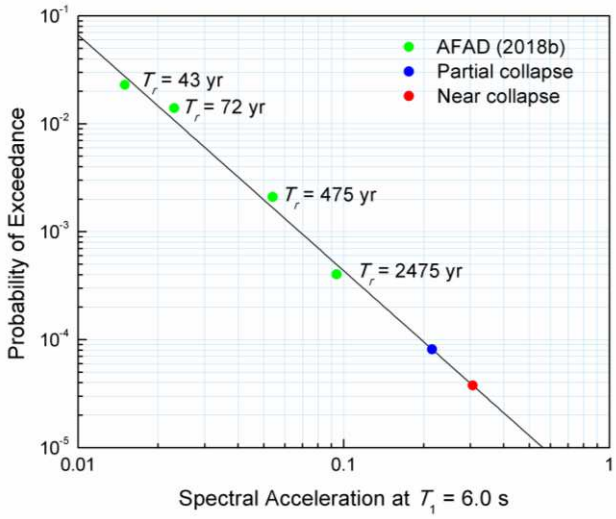

Fig. 16 Seismic hazard curve for the building site

10 Discussion and conclusions

The investigated tall building, designed according to performance-based design principles as outlined, displays remarkable seismic performance. It remains linear elastic under the SLE, and displays limited damage performance under the MCE ground motions. Significant inelastic actions occur only at the coupling beams and particular sections of the core walls where ductile flexural response is ensured.

Service performance level is either controlled by the force response of coupling beams expressed in terms of DCR limits in the regions of low wind speeds, or maximum IDR limits specified for wind loads in the regions of high wind speeds. Safety and partial collapse limit states are controlled by the flexural response limits of coupling beams whereas near collapse limit state is controlled by the concrete strain limits at the confined shear wall end regions. Perimeter columns and outrigger struts do not undergo inelastic action under the SLE, which conform to the basic design objectives.

The basic reason behind such favorable seismic performance is the overstrength in design, primarily due to the limitation of axial forces in vertical members. The outrigger trusses employed for deformation control under wind loading also contribute to overstrength, although to a lesser extent. An overstrength ratio can be defined in both directions, as the maximum ratio of the MCE to SLE base shear demands from Fig. 10. These are 5.8 and 4.6 in the X and Y directions, respectively. Both factors are about twice the overstrength factors suggested in ASCE 7-16 (ASCE 2017) for ordinary concrete buildings.

The inherent overstrength in seismic design reduces the damage risk and increases the seismic performance significantly. The annual frequency of the mean earthquake ground motions that will lead to collapse reduces from the target value of $4 \cdot 10^{-4}$ (1/2475) defined for the MCE for ordinary buildings, to $8 \cdot 10^{-5}$ (1/12000) for partial collapse, and to $4 \cdot 10^{-5}$ (1/27000) for near collapse of the tall core wall building. However, this safety increase cannot be regarded as a waste of resources. It comes at a cost that can be considered negligible when compared to the large investment cost of a tall building. It has to be considered that tall buildings, which are designed to meet the current performance based guidelines, have not yet been tested under extreme earthquake ground motions.

Declarations

Funding

No funding was received for this research.

Acknowledgments

The authors thank Professors Sinan Akkar and Erkan Ozer for discussing design details as peer reviewers of the design, Professor Bekir Ozer Ay for ground motion selection, and Design Group Inc. for providing design data.

References

ACI (2014) Building code requirements for structural concrete, ACI 318-14. American Concrete Institute, Farmington Hills, Michigan

AFAD (2018a) Turkish earthquake code for buildings. Disaster and Emergency Management Authority, Ankara, Turkey

AFAD (2018b) Seismic hazard maps of Turkey. Disaster and Emergency Management Authority, Ankara, Turkey. https://tdth.afad.gov.tr. Accessed 14 January 2022

Akkar S (2014) Site-specific probabilistic hazard assessment to compute elastic response spectra of 43-year, 475-year and 2475-year return periods for Istanbul Tower 205 project and corresponding scaled ground motions, Report. Istanbul, Turkey

Arup Inc. (2013) Conceptual design report of Istanbul Tower 205. Istanbul, Turkey

ASCE (2012) Wind tunnel testing for building and other structures, ASCE/SEI 49-12. American Society of Civil Engineers, Reston, Virginia

ASCE (2014) Seismic evaluation and retrofit of existing buildings, ASCE/SEI 41-13. American Society of Civil Engineers, Reston, Virginia

ASCE (2017) Minimum design loads and associated criteria for buildings and other structures, ASCE/SEI 7-16. American Society of Civil Engineers, Reston, Virginia

Bilotta A, Tomeo R, Nigro E, Manfredi G (2018) Evaluation of the seismic demand of an existing tall building. Ingegneria Sismica 35(1):67-87

Budak E, Sucuoğlu H, Konca F, Uludağ A (2018) Performance based seismic evaluation of a 62 story RC tower in Istanbul. 16th European Conference on Earthquake Engineering, Thessaloniki

Cornell CA, Jalayer F, Hamburger RO, Foutch DA (2002) Probabilistic basis for 2000 SAC Federal Emergency Management Agency steel moment frame guidelines. Journal of Structural Engineering, ASCE 128(4):526–533

CSI (2011) ETABS version 9.7.4, Building analysis and design. Computers and Structures Inc., Walnut Creek, California

CSI (2016) Perform3D version 6.0, Performance-based design of 3D structures. Computers and Structures Inc., Walnut Creek, California

Erdik M, Aydinoglu N, Fahjan Y et al (2003) Earthquake risk assessment for Istanbul metropolitan area. Earthquake Engineering and Engineering Vibration 2(1):1–23

European Committee for Standardization (2005) Eurocode 1: Actions on structures, EN 1991-1-4. Brussels, Belgium

FEMA (2020) NEHRP recommended seismic provisions for new buildings and other structures, FEMA P-2082-1. Federal Emergency Management Agency, Washington, D.C.

Korista DS, Sarkisian MP, Abdelrazaq A (1997) Jin Mao Tower - Shanghai response of an ultra-tall building to moderate seismic forces. In: Proceedings of the Fourth Conference on Tall Buildings in Seismic Regions, Los Angeles, California, pp 171-186

LATBSDC (2017) An alternative procedure for seismic analysis and design of tall buildings located in the Los Angeles region. Los Angeles Tall Buildings Structural Design Council, Los Angeles, California

Lowes LN, Lehman DE, Baker C (2016) Recommendations for modeling the nonlinear response of slender reinforced concrete walls using PERFORM-3D. In: SEAOC Convention. Maui, Hawaii

Mander JB, Priestley MJN, Park R (1988) Observed stress-strain behaviour of confined concrete. Journal of Structural Engineering, ASCE 114(8):1827–1849

Moehle JP, Ghodsi T, Hooper JD, Fields DC, Gedhada R (2012) Seismic design of cast-in-place concrete special structural walls and coupling beams, NIST GCR 11-917-11REV-1. National Institute of Standards and Technology, Gaithersburg, Maryland

MPWS (2007) Specification for buildings to be built in seismic zones. Ministry of Public Works and Settlement, Ankara, Turkey

Odabasi O, Kohrangi M, Bazzurro P (2021) Tall buildings in Turkey, their characteristic structural features and dynamic behavior. Bulletin of Earthquake Engineering 19:2105–2124

PEER (2010) Modeling and acceptance criteria for seismic design and analysis of tall buildings, PEER/ATC 72-1. Pacific Earthquake Engineering Research Center, Richmond, California

PEER (2017) Guidelines for performance-based seismic design of tall buildings, PEER Report No. 2017/06. Pacific Earthquake Engineering Research Center, Berkeley, California

PEER (2022) PEER Ground Motion Database. Pacific Earthquake Engineering Research Center. http://ngawest2.berkeley.edu. Accessed 14 January 2022

Pugh JS, Lowes LN, Lehman DE (2015) Nonlinear line-element of flexural reinforced concrete walls. Engineering Structures 104:174–192

SEAONC (2007) Recommended administrative bulletin on the seismic design and review of tall buildings using non-prescriptive procedures, AB-083. Structural Engineers Association of Northern California, San Francisco, California

Smith R (2011) Deflection limits in tall buildings—are they useful? In: Structures Congress. Las Vegas, Nevada, pp 515–527

TSI (2000) Requirements for design and construction of reinforced concrete structures, TS 500. Turkish Standards Institute, Ankara, Turkey

Wallace JW (2007) Modeling issues for tall reinforced concrete core wall buildings. The Structural Design of Tall and Special Buildings 16:615–632

Wang LJ, Lai JW, Schoettler MJ, Mahin SA (2017) Seismic assessment of existing tall buildings: A case study of a 35-story steel building with pre-Northridge connection. Engineering Structures 141:624–633

WTG (1996) Windkanaluntersuchungen in der Gebaudeaerodynamik, Windtechnologische Gesellschaft (in German)

Zekioglu A, Willford M, Jin L, Melek M (2007) Case study using the Los Angeles tall buildings structural design council guidelines: 40-storey concrete core wall building. The Structural Design of Tall and Special Buildings 16:583–597